Thermal cycling test in Sn-Bi and Sn-Bi-Cu solder joints

HUI-WEI MIAO, JENQ-GONG DUH
Department of Materials Science and Engineering, National Tsing Hua University, Hsinchu, Taiwan

BI-SHIOU CHIOU
Department and Institute of Electronics Engineering, National Chiao Tung University, Hsinchu, Taiwan
E-mail: jgd@mse.nthu.edu.tw

The eutectic SnBi solder alloy is a candidate for Pb-free replacement of the conventional eutectic SnPb solders. This study presents series of results on the binary eutectic SnBi and ternary SnBi-1 wt % Cu a solder joints. Compositional analysis and wettability of the as-fabricated solder alloys are reported. In addition, microstructure, adhesion strength, fracture surface and contact resistance of the solder joints are also evaluated. The results of the wetting balance show that the addition of 1 wt % Cu has little effect on the contact angle of the eutectic SnBi solder alloy with various metallization layers. The adhesion strength of solder joints degrades abruptly after 2000 thermal cycles. In addition, thermal cycling would result in cracking in the solder joints, which is due to the mismatch in thermal expansion coefficients. Portions of the thermal fatigue cracks nucleate at the edge of the solder fillet, and then propagate along the solder/conductor interface. Some cracks are, however, through the Al_2O_3 substrate. The contact resistance of the solder/Cu joint does not increase after thermal cycling since the resistivity of Cu_6Sn_5 is lower than that of the solder. The solder joints of 42Sn-58Bi/Cu, SnBi-1Cu/Cu, 42Sn-58Bi/PtAg, and SnBi-1Cu/PtAg assemblies maintain their integrity after 2000 thermal cycles since the increase in contact resistance is rather small ($\Delta R < 0.5\,m\Omega$).
© *2000 Kluwer Academic Publishers*

1. Introduction

Soldering technology plays a key role in various levels of electronic packaging since solders are commonly used in the electronic industry to join components. In fact, the solder joint is an essential part of electronic devices for it acts not only as an electrical connection but also as a mechanical bond [1, 2]. Nowadays, solder joints with higher reliability are demanded because the trend in electronic packages is to make products smaller and faster. The reliability of solder joints is dependent on solder composition, soldering condition, and joint geometry [3]. With appropriate joint design, the use of solder alloys with excellent properties, and the employment of a better process, reliable joints are obtained.

The eutectic SnPb alloys are the most widely used solder material today due to their well-known and excellent properties [1, 4–7]. However, there are environmental and health concerns about the toxicity of Pb in the SnPb solder alloys [4–6, 8–14]. Because of these concerns, there has been a great deal of research in recent years to develop alternative Pb-free solders. During soldering, a considerable strain is produced in the board [15]. Fortunately, the residual strain may be reduced by using a lower melting point solder. The eutectic SnBi alloy is a possible Pb-free solder for low temperature soldering due to its low melting temperature. When devices to be soldered are prone to thermal damage, low temperature soldering is necessary [4, 16]. Low temperature soldering can also reduce the damage of thermal cycling caused by thermal expansion mismatch among various materials in an electronic package [16]. Another application of low temperature soldering is step soldering, which is applied when soldering requires more than one step. The melting point of the solder used in a subsequent step should be lower than that of solder used in the previous step [11, 16].

The tensile strength of the eutectic SnBi solder is higher than that of the eutectic SnPb solder [1, 15]. In addition, the 42Sn-58Bi solder has a better creep resistance than the eutectic Sn-Pb solder [1, 8, 17]. However, the 42Sn-58Bi solder alloy exhibits noticeable microstructure coarsening during thermal aging [8–10, 14, 17]. The microstructure instability at elevated temperature has can be suppressed by incorporating finely dispersed particles into the eutectic SnBi solder alloys [8, 9, 14, 17].

Solder joint failure under thermal cycling has been one of the most critical problems in microelectronic package

technology. In order to ensure high reliability, it is critical to characterize the thermal cycling performance of the solder joint. The effect of thermal aging on a Sn-Ag solder joint was recently reported by Wei and Duh [18]. The purpose of this study is first to investigate the wettability of as-fabricated binary Sn-Bi and ternary Sn-Bi-Cu solders. Various solder joints were derived with the as-fabricated solders coupled with different metallized substrates, and then subjected to a series of thermal cycling tests. The effect of the thermal cycling on the microstructure and mechanical properties of solder joints was probed. In addition, the electrical resistance of joints under thermal cycling was evaluated.

2. Experimental procedures

2.1. Fabrication of solder alloys

The eutectic SnBi and the SnBi-1 wt % Cu solder alloys were fabricated from raw materials including pure tin, pure bismuth (purity > 99.9%, Chung-Cheng Inc., Taiwan), and pure copper (purity > 99.9%, High Purity Chemical Research Center, Japan). Raw materials with appropriate weight were cleaned and put into a quartz tube evacuated to 1×10^3 Pa. The tube was then placed in a furnace at 1050 °C for 8 h and continuously rotated during melting for the purpose of homogenization. Finally, the tube was taken out and quenched into cold water. The solder alloys were then obtained after the tube was broken.

2.2. Pretreatment of the conductor/Al_2O_3 coupons

Metallized substrates including PtAg/Al_2O_3 and Cu/Al_2O_3 assemblies with various pattern configurations were supplied by ERSO (Electronics Research and Service Organization, Hsinchu, Taiwan), as illustrated in Fig. 1. The thicknesses of the PtAg and Cu conductors, measured with an α-step, were 10 μm and 15–20 μm, respectively. The conductor/Al_2O_3 coupons were then cleaned ultrasonically in alcohol and acetone for 5 min, respectively.

2.3. Soldering process

2.3.1. Solder paste/conductor/FR4 joint

The commercial eutectic 42Sn-58Bi solder paste consisting of 88 wt % and 12 wt % RMA flux (Indium Corporation of America, U.S.A.) was used. Two kinds of metallizations with the FR4 substrates were employed, including Cu and Au/Ni/Cu conductors. When capacitors (1206 LCCC) were soldered onto Cu conductors with a temperature-controled soldering iron (TS-316, Tonica, Taiwan), 8-pin SMDs were soldered onto Au/Ni/Cu conductors. The soldering temperature was 200 °C. Schematic diagrams of the soldered joints are shown in Fig. 2.

2.3.2. As-fabricated solder/conductor/Al_2O_3 joint

Two soldering steps were conducted in the as-fabricated solder/conductor/Al_2O_3 joint. First, joints of (Cu conductor)/(Al_2O_3 substrates) and (PtAg conductor)/(Al_2O_3 substrates) were dipped into a bath of molten solders maintained at 200 °C. Next, the hot-dipped coupons were reflowed on a temperature-controled hot plate at 200 °C. At the same time, the capacitors were applied on the hot-dipped coupons. Finally, solder joints were formed after air cooling. A schematic diagram of the soldered assembly is indicated in Fig. 2.

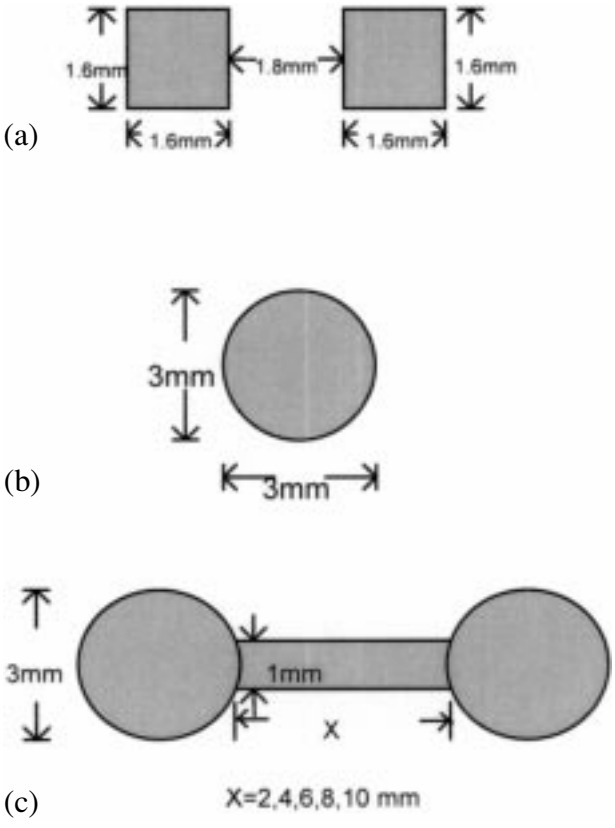

Figure 1 Configurations of pattern with the PtAg and Cu conductors (a) for contact resistance measurement, (b) for soldering with 1206 LCCC capacitor, (c) for pull-off test.

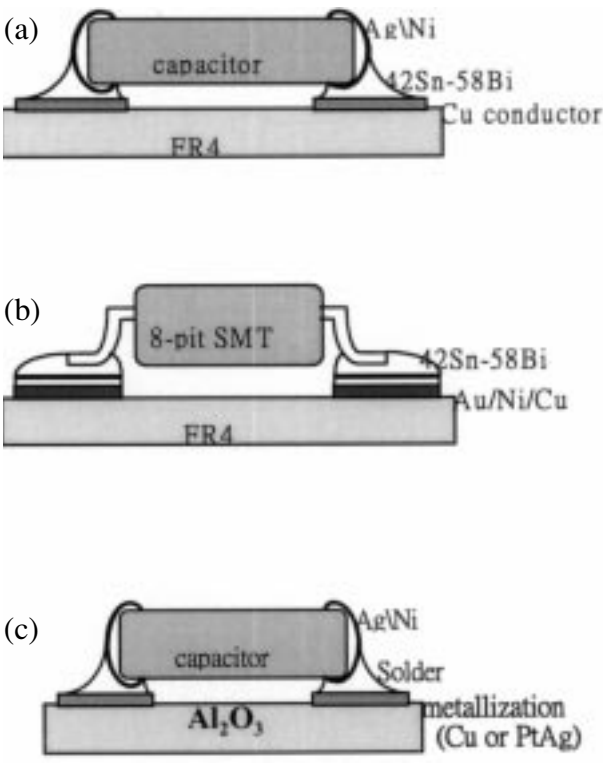

Figure 2 Schematic diagram of the soldered coupons.

2.4. Thermal cycling

Soldered joints were exposed to accelerated thermal cycling from $-55\,^{\circ}C$ to $100\,^{\circ}C$ at a ramp rate of $30^{\circ}C\ min^{-1}$, and 30 min dwell. A block diagram of the actual thermal shock profile is shown in Fig. 3. The testing was interrupted after every 250 cycles to remove several modules for subsequent analysis.

2.5. Analysis and test

2.5.1. X-ray diffraction

The phase and crystal structure of the as-fabricated solder alloy and the soldered assembly were identified with an X-ray diffractometer (D/MAX-B, Rigaku, Japan) with a wavelength of CuK_{α} ($\lambda = 0.15406$ nm). The scanning rate was $4^{\circ}\ min^{-1}$.

2.5.2. Wettability test

The wetting angles of different solder alloys on various metallized substrates were characterized with a wetting balance (ST50, Metronelec, France). The sample was suspended from a sensitive spring system and immersed edgewise to a predetermined depth in a molten solder at a controlled temperature within $\pm 2\,^{\circ}C$. The resultant vertical forces of buoyancy and surface tension acting on the immersed sample were recorded as a function of time on a high-speed chart recorder.

2.5.3. SEM and EPMA

The morphology and elemental distribution of the specimens were analyzed with a scanning electron microscope (SEM, JEOL 840A, Japan) and an electron probe microanalyzer (EPMA, JXA-8800M, JEOL, Japan), respectively. In addition, the compositions of the as-fabricated solder alloy were quantitatively measured by EPMA.

2.5.4. ICP-AES test

The composition of the minor element, i.e., Cu, in the as-fabricated ternary solder alloys was measured by inductively coupled plasma-atomic emission spectrometry (ICP-AES) (ICAP 9000, Jarrell-Ash, USA).

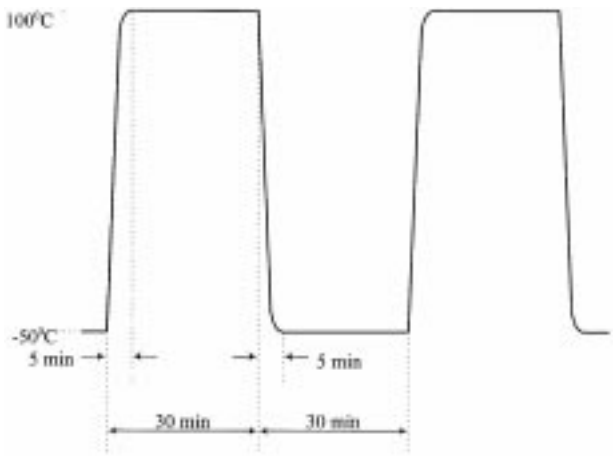

Figure 3 Block diagram of the actual thermal shock profile.

2.6. Adhesion strength measurement

The adhesion strength of the soldered assembly was evaluated with a direct pull tester (SEBASTIAN FIVE, QUAD Group, USA). A stud was bonded perpendicular to the substrate surface. The tester pulled the stud down against the platen support ridge until the solder joint failed. A schematic diagram of the pull-off test is illustrated in Fig. 4.

2.7. Contact resistance measurement

The contact resistance of the solder/base metal interface was measured with an ohm meter (502A, Chen Hwa, Taiwan). The pattern used to measure the resistance is shown in Fig. 1c.

3. Results and discussion

3.1. Characteristics of the as-fabricated solder alloys

3.1.1. Solder compositions

The as-fabricated 42Sn-58Bi and SnBi-1Cu solder alloys were investigated by two methods, i.e., ICP-AES and EPMA, to evaluate the compositions. Table I lists the results of quantitative analysis. The compositions in the binary alloy measured by EPMA are 42.4 ± 0.43 wt % Sn and 57.6 ± 0.43 wt % Bi. In the binary Sn-Bi phase diagram, the composition of the eutectic SnBi solder is 42 wt % Sn and 58 wt % Bi. Thus, the as-fabricated binary solder can be considered to possess a eutectic composition within experimental error. In addition, the composition of the as-fabricated ternary solder alloy measured by EPMA is 43.41 ± 1.70 wt % Sn, 55.74 ± 1.69 wt % Bi, and 0.85 ± 0.10 wt % Cu. Moreover, the content of the minor element (copper) in the ternary solder alloy measured with ICP-AES is 0.92 ± 0.06 wt %. It is apparent that the compositions of the as-fabricated solder are fairly close to the nominal one.

3.1.2. Evaluation of wettability

The contact angles between solders (42Sn-58Bi and SnBi-1Cu alloys) and the metallized substrate are evaluated with a wetting balance. During the wetting process, the drop of interfacial energy caused by the interfacial reaction brings about the lowering of the contact angle. A few seconds are usually needed to achieve a stable contact angle. In addition to contact

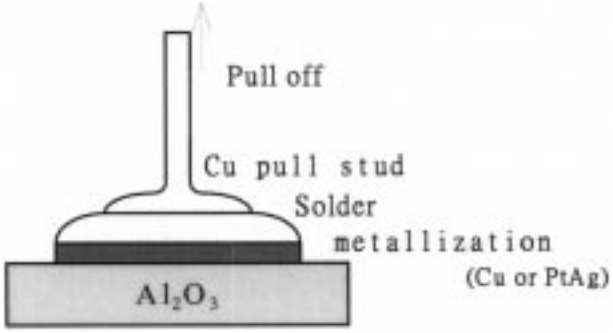

Figure 4 Schematic diagram of the pull-off test.

TABLE I Compositions of as-fabricated 42Sn-58Bi and SnBi-1Cu solder alloys by EPMA and ICP Analysis

Alloy	Sn (wt %)	Bi (wt %)	Cu (wt %)	Remarks
Binary eutectic SnBi	42.40 ± 0.43	57.60 ± 0.43		EPMA
Ternary SnBi-1Cu	43.41 ± 1.70	55.74 ± 1.69	0.85 ± 0.10	EPMA
Ternary SnBi-1Cu			0.92 ± 0.06	ICP

angle, the time of the contact angle becoming stable is another index of wettability. It is observed that the wetting time of solders on Ni foil is longer than that of solders on other metallizations, possibly due to the fact that the reactivity of Ni is lower than other base metals since Ni is usually used as a diffusion barrier. In fact, the wetting behavior is influenced by solder composition, metallization, soldering temperature, flux utilization, and surrounding atmosphere. The results measured in this study are indicated in Table II. The data shows that the addition of 1.0 wt % Cu has little effect on the wetting properties of the eutectic SnBi solder alloy. This result is encouraging because adding 1.0 wt % copper to the 42Sn-58Bi solder would not degrade the wettability on most metallized substrates.

3.2. Thermal cycling test

3.2.1. Location of cracks

Figs 5 and 6 exhibit the micrographs of the 42Sn-58Bi/Cu/FR4 and the 42Sn-58Bi/Ni/Cu/FR4 solder joints after 0, 500, 1000, 1500, 2000 thermal cycles, respectively. A crack is found at the solder/Ni interface after 1500 cycles, while no crack is observed in the 42Sn-58Bi/Cu/FR4 assembly even after 2000 cycles. It is argued that this discrepancy is attributed to the similar thermal expansion coefficients among the eutectic SnBi solder, Cu, and FR4, as compared to the dissimilar CTE of Ni. The thermal expansion coefficients of materials in the current study used are given in Table III.

It is generally believed that cracks are caused by stress concentration in the solder joint. The difference in the thermal expansion coefficients of various materials causes joint failure during thermal cycling. In addition, the geometry of the solder joint is another factor which influence the joint's failure [19]. The mismatch of thermal expansion coefficients causes stress, and the joint geometry determines where the stress is concentrated. Simulations using a finite element model (FEM) for the leaded and unleaded solder joints have been illustrated in the literature [20]. During thermal cycling, the highest stress was concentrated in the heel and toe fillet of the leaded joint, while stress concentrates at the edge of the solder fillet of the unleaded joint. It is evident that the location of the observed cracks as shown in Figs 5 and 6 is in agreement with that by FEM simulation.

The micrographs of the 42Sn-58Bi and the SnBi-1Cu solders in the Cu/Al_2O_3 and the $PtAg/Al_2O_3$ coupons after 1500 cycles are shown in Fig. 7. The cracks found in the joint are still small after 1500 cycles while no crack is observed before 1500 cycles. Cracks nucleate at the edge of the solder fillet and then propagate along the solder/conductor interface since the interface is a weaker region of solder joints. Yao and Shang [21] also reported that the growth of a thermal fatigue crack was along the interface between the solder and the conductor. The fact that a crack occurs earlier in the solder/Cu/Al_2O_3 joint than in the solder/Cu/FR4 joint is due to the larger CTE mismatch between solder/Cu and the Al_2O_3 substrate. In addition, some cracks are observed in the Al_2O_3 substrate, as shown in Fig. 8. The thermal cycling induced substrate cracking phenomenon was also reported by Keusseyan and co-workers [23, 24], who has indicated that these cracks are attributed to stress concentration and the brittle nature of the ceramic substrate.

TABLE II Contact angle of SnBi and SnBi-1Cu solder alloys on different metal foils and metallized substrates

	SnBi	SnBi-1Cu
Au foil	45.8° ± 5.0°	46.2° ± 3.4°
Ag foil	51.3° ± 3.7°	44.8° ± 4.4°
Ni foil	57.6° ± 6.6°	67.2° ± 5.5°
Cu foil	48.5° ± 9.8°	56.4° ± 6.4°
Cu thick film/FR4	36.0° ± 6.2°	35.2° ± 5.9°
Cu thick film/Al_2O_3	37.0° ± 3.4°	35.4° ± 5.3°
PtAg thick film/Al_2O_3	55.3° ± 3.0°	47.1° ± 7.1°

3.2.2. Mechanical property and fracture surface of the solder joint

To characterize the location where the fracture occurs, the fracture mode of the pull-off test is categorized as follows:

1. A mode: failure at the pull-stud/solder interface.
2. B mode: failure at the solder/conductor interface.
3. C mode: failure at the conductor/substrate interface.
4. D mode: failure in the copper pull stud.
5. E mode: failure occurred inside the substrate.

The different types of fracture mode indicate different locations where the fracture would occur. In practice, most joints are not fractured with a pure single mode, and the criterion to classify the fracture area is then described as follows. If the solder/conductor interface fracture area is larger, then it is B mode fracture. If the conductor/substrate interface area is dominant, then the C mode is specified.

The adhesion strength and the fracture mode in the eutectic SnBi and the SnBi-1Cu solder alloys on Cu/Al_2O_3 and $PtAg/Al_2O_3$ assemblies after thermal cycling are presented in Tables IV–VII. It is apparent that the adhesion strength of the joint decreases after thermal cycling. It should be pointed out that all joints show no appreciable strength degradation until 2000 thermal

TABLE III Thermal expansion coefficients of various materials

Materials	CTE at 20 °C (ppm °C^{-1})	Ref.
42Sn-58Bi	15	[10, 16]
Cu	16.5	[25]
Ni	13.3	[25]
Ag	19.68	[25]
FR4(X–Y plane)	17.7	[26]
Al_2O_3	7.1	[2]

cycles. As presented in the previous section, cracks in the solder joint are found after 1500 cycles, and the cracks are still small in size at this time. Since cracks grow as thermal cycling continues, strength degradation occurs when cracks have grown beyond a critical size to destroy the joint. The occurrence of E mode fracture is caused by stress concentration and the brittle nature of the Al_2O_3 substrate [23, 24]. According to the FEM simulation for the solder joint, stress concentrates at the edge of the solder filler [20]. Since the CTE of the Al_2O_3 substrate is very different from that of other materials and also Al_2O_3 is quite brittle, the concentrated stress may be released by the formation of microcracks. As the number of thermal cycles increases, microcracks are enhanced in number and length. Eventually, apparent macrocracks are observed, as illustrated in Fig. 8. The fracture surface in the Al_2O_3 substrate is shown in Fig. 9.

3.3. Electrical measurement

In order to assess the performance of ohmic contacts to semiconductors, the contact resistance of the solder joint is measured. The pattern given in Fig. 1 is designed to measure the contact resistance of the solder joints. With various lengths between the two joints, contact resistance is obtained by interpolation, as illustrated in Figs 10 and 11. Contact resistance is dependent on many variables, such as the amount and composition of intermetallics and the site, length, and conducted path of cracks. Fig. 12 shows the contact resistance as a function of number of cycles. In addition, the increased percentage of contact resistance as a function of number of cycles is also presented in Fig. 13. The contact resistance of SnBi-1Cu/Cu, 42Sn-58Bi/PtAg, and SnBi-1Cu/PtAg interfaces increases slightly after 2000 thermal cycles, while that of the 42Sn-58Bi/Cu joint is not altered (Fig. 12).

It should be pointed out that the error in the measurement of the contact resistance in Fig. 12 was around several per cent of the measured value. Usually the error was less than 3%, with some exceptions around 5%. In Fig. 13, there is essentially no significant change of contact resistance in the 42Sn-5SBi/Cu joint. For the SnBi-1Cu/Cu joint, the change is less than 5% after 1500 cycles. However, it is close to 10% after 1500 cycles for the SnBi-1Cu/PtAg joint. Relatively, the contact resistance exhibits a significant increase only in the 42Sn-

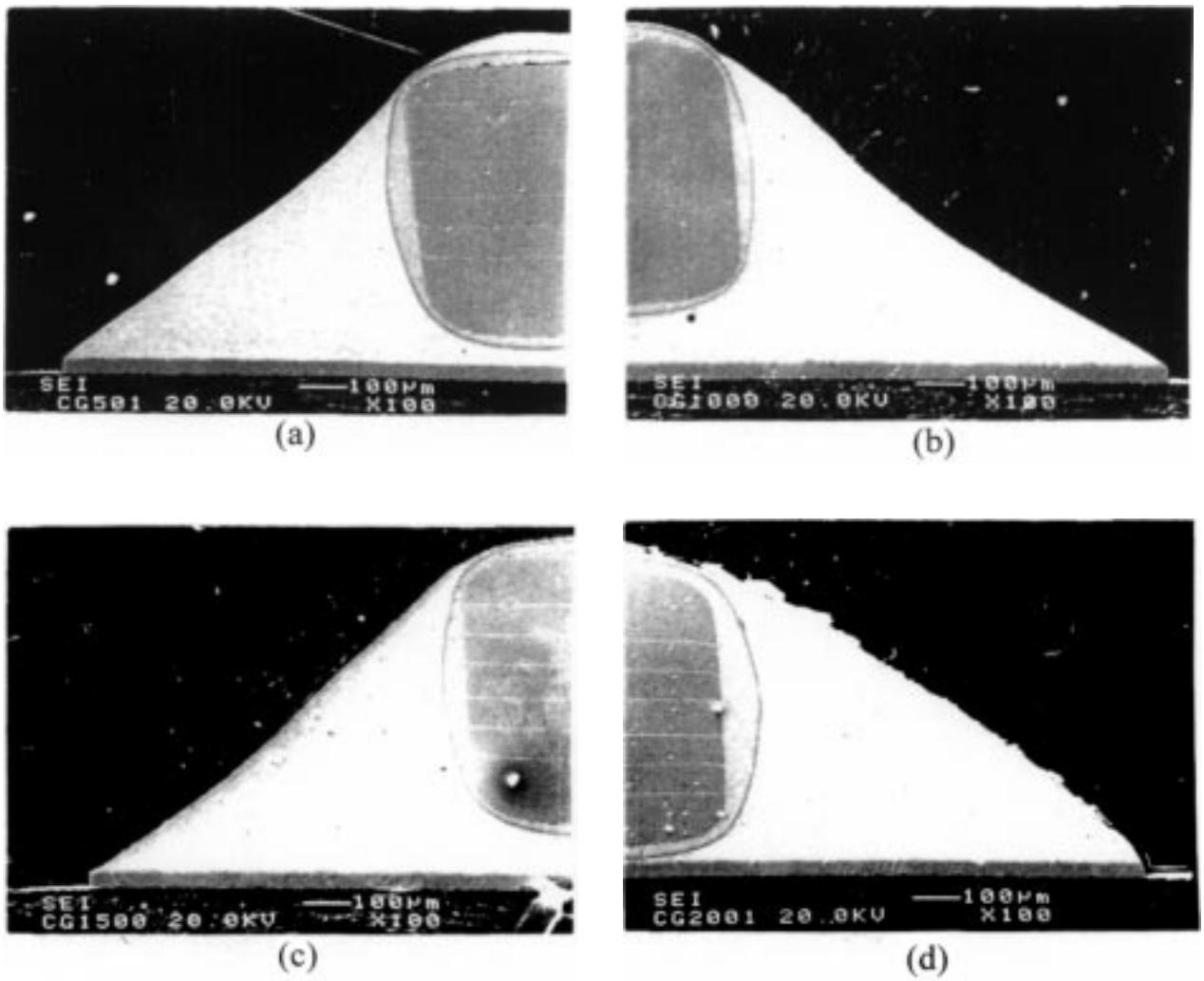

Figure 5 Micrographs of the 42Sn-58Bi/Cu/FR4 joint after (a) 500, (b) 1000, (c) 1500, and (d) 2000 thermal cycles.

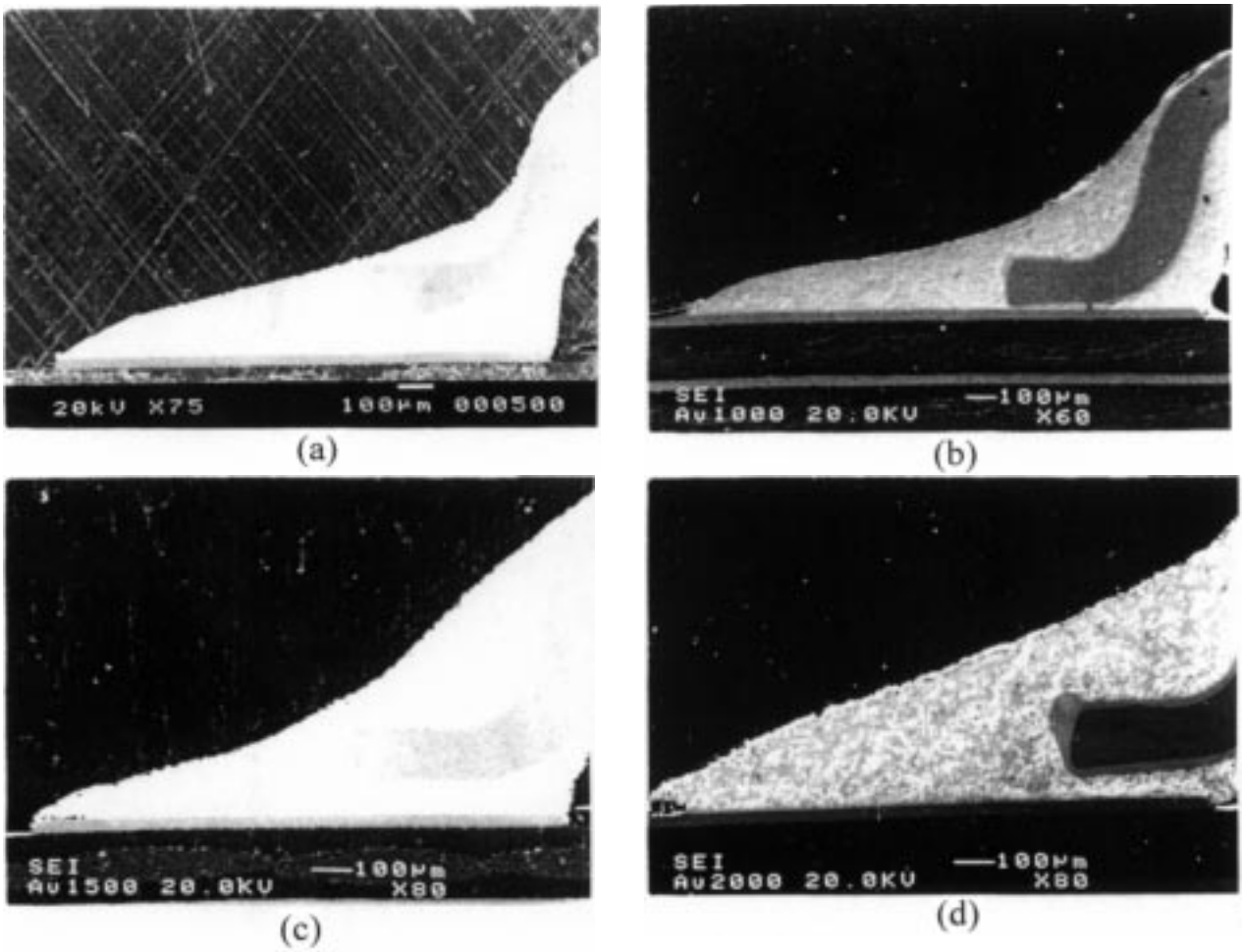

Figure 6 Micrographs of the 42Sn-58Bi/Cu/Ni/FR4 joint after (a) 500, (b) 1000, (c) 1500, and (d) 2000 thermal cycles.

58Bi/PtAg joint. Although there is some increase in the contact resistance of the joint after thermal cycles, the amount of increase is relatively small.

The change in contact resistance of the solder/PtAg joint after thermal treatment could result from the growth of intermetallics and cracks. Usually, a slight increase in contact resistance would still result in enhancement of dissipated heat, and degradation of the solder joint. Nevertheless, the increase in the measured contact resistance is quite small ($\Delta R < 0.5\,\text{m}\Omega$). It is believed that solder joints of the 42Sn-58Bi/Cu, SnBi-1Cu/Cu, 42Sn-58Bi/PtAg, SnBi-1Cu/PtAg in the current study retain the integrity and prevail after 2000 thermal cycles.

TABLE IV Adhesion strength (kg/cm^{-2}) of the 42Sn58Bi/Cu joint with corresponding fracture mode after thermal cycling

Fracture mode	Number of Thermal cycle					
	250	500	750	1000	1500	2000
A	(2/8)* 662 ± 42					
B	(3/8) 726 ± 24	(7/10) 717 ± 63	(5/6) 599 ± 46	(7/8) 669 ± 25	(4/6) 618 ± 28	(4/5) 164 ± 37
E	(1/8) 774	(1/10) 170	(1/6) 174	(1/8) 159		(1/5) 44
D	(2/8) 864 ± 9	(2/10) 838 ± 23			(2/6) 856 ± 3	

*The denominator indicates the number of the overall test while the numerator is the number of samples fractured with specifical fracture mode.

TABLE V Adhesion strength (kg cm^{-2}) of the SnBi-1Cu/Cu joint with corresponding fracture mode after thermal cycling

Fracture mode	Number of thermal cycle					
	250	500	750	1000	1500	2000
A						
B	(4/7) 804 ± 39	(5/11) 721 ± 34	(3/4) 547 ± 36	(3/7) 516 ± 31	(1/5) 548	(1/4) 236
E		(6/11) 175 ± 52	(1/4) 107	(4/7) 164 ± 53	(3/5) 196 ± 77	(3/4) 83 ± 19
D	(3/7) 869 ± 2					

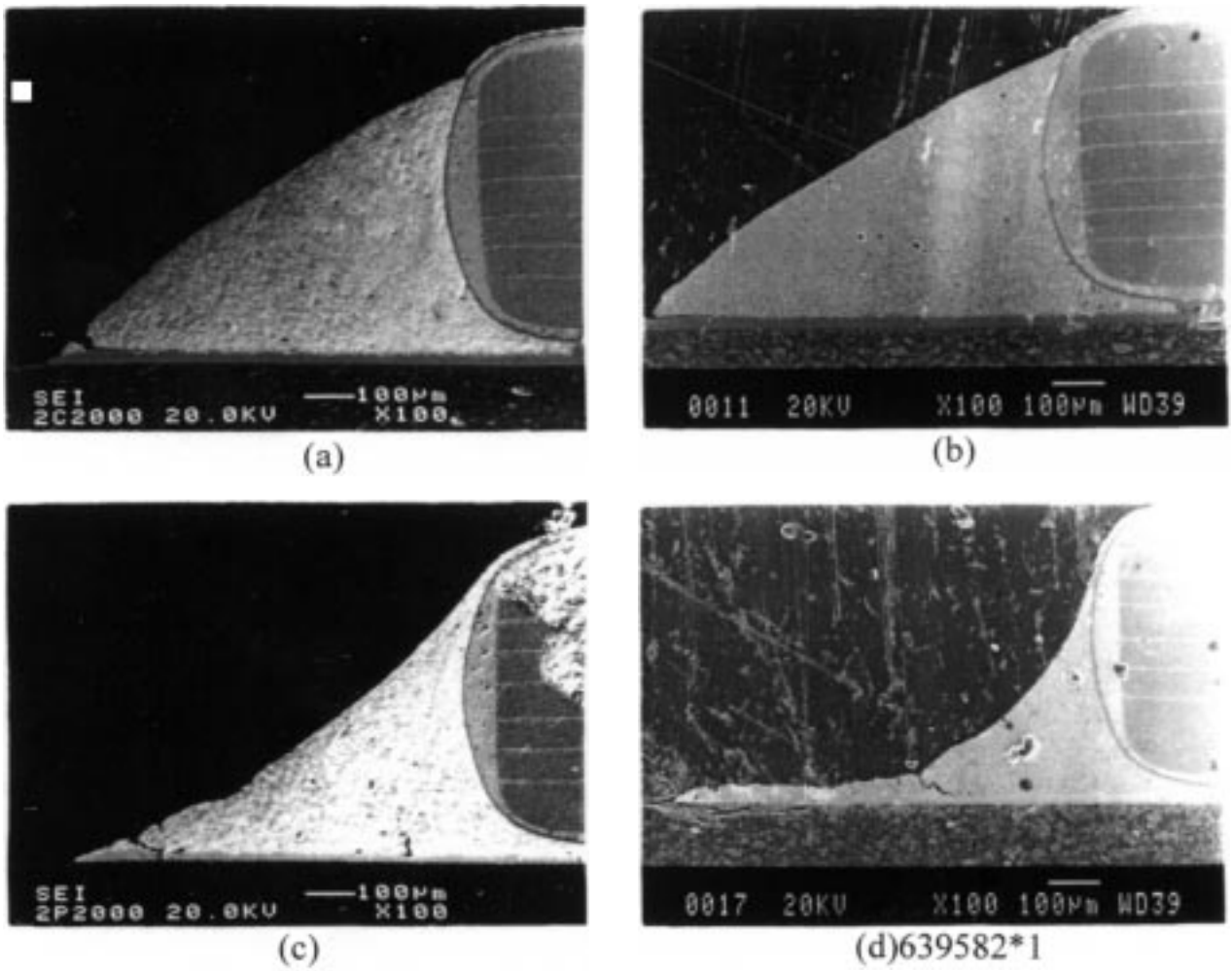

Figure 7 Micrographs of the (a) 42Sn-58Bi/Cu/Al_2O_3, (b) SnBi-1Cu/Cu/Al_2O_3, (c) 42Sn-58Bi/PtAg/Al_2O_3 and (d) SnBi-1Cu/Pt-Ag/Al_2O_3 joints after 1500 thermal cycles.

4. Conclusions

1. The binary 42Sn-58Bi and ternary SnBi-1Cu solder alloys have been fabricated, and coupled with various metallized substrates to be employed as solder joints to test the reliability under thermal cycling. Wettability tests show that the addition of 1 wt % copper has negligible influence on the contact angle of the eutectic SnBi solder alloy.

2. Various fracture modes are characterized for solder joints after thermal cycle tests. The adhesion strength of solder joints degrades abruptly after 2000 thermal cycles, during which cracks result due to the mismatch of

TABLE VI Adhesion strength ($kg\,cm^{-2}$) of the 42Sn58Bi/PtAg joint with corresponding fracture mode after thermal cycling

Fracture mode	Number of thermal cycles					
	250	500	750	1000	1500	2000
A	(1/5) 646					
B	(1/5) 669	(2/11) 607 ± 51	(2/5) 631 ± 14	(1/7) 513	(4/7) 669 ± 53	(2/5) 187 ± 35
E	(2/5) 179 ± 70	(9/11) 182 ± 82	(3/5) 167 ± 71	(6/7) 174 ± 73	(3/7) 124 ± 36	(3/5) 89 ± 24
D	(1/5) 866					

TABLE VII Adhesion strength ($kg\,cm^{-2}$) of the SnBi-1Cu/PtAg joint with corresponding fracture mode after thermal cycling

Fracture mode	Number of thermal cycles					
	250	500	750	1000	1500	2000
A	(1/5) 730					
B		(1/6) 766	(1/5) 721	(1/5) 504	(2/4) 465 ± 44	(2/4) 226 ± 31
E	(4/5) 118 ± 18	(5/6) 111 ± 8	(4/5) 102 ± 11	(4/5) 89 ± 20	(2/4) 116 ± 7	(2/4) 86 ± 38
D						

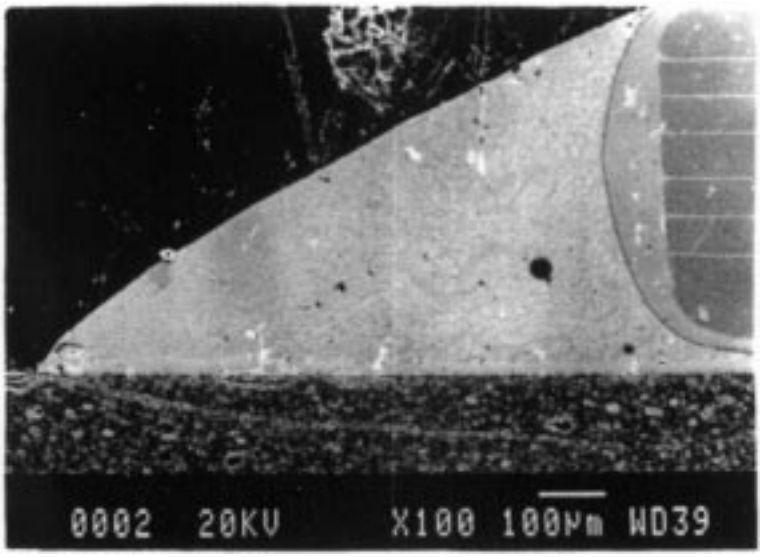

Figure 8 Crack observed in solder/PtAg/Al_2O_3 joint, propagates down to the Al_2O_3 substrate.

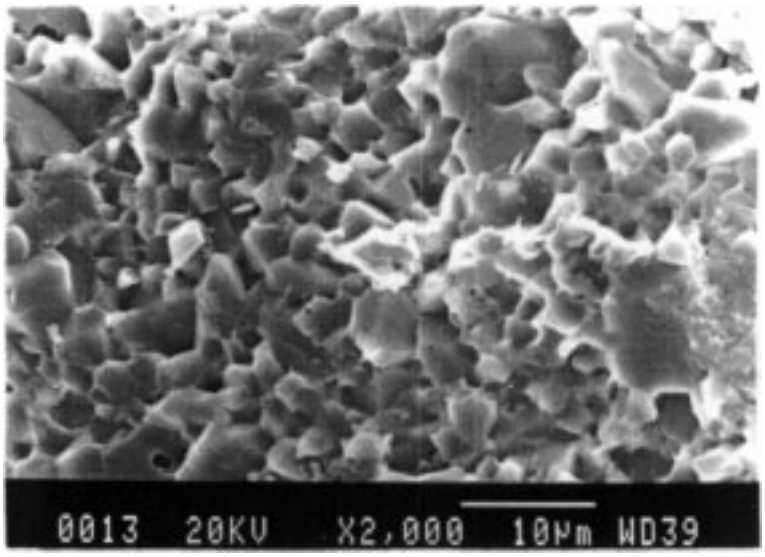

Figure 9 Micrograph of the fracture surface in Al_2O_3 substrate.

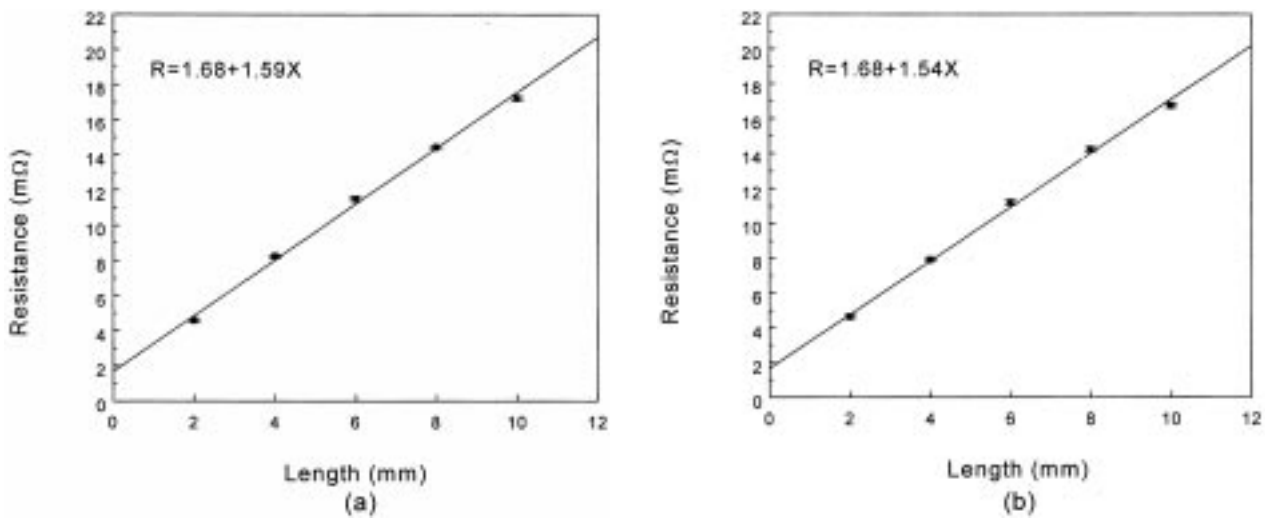

Figure 10 Resistance of various solder joints (a) 42Sn-58Bi/Cu, (b) SnBi-1Cu/Cu joint versus different length, which is indicated as X in Fig. 1a.

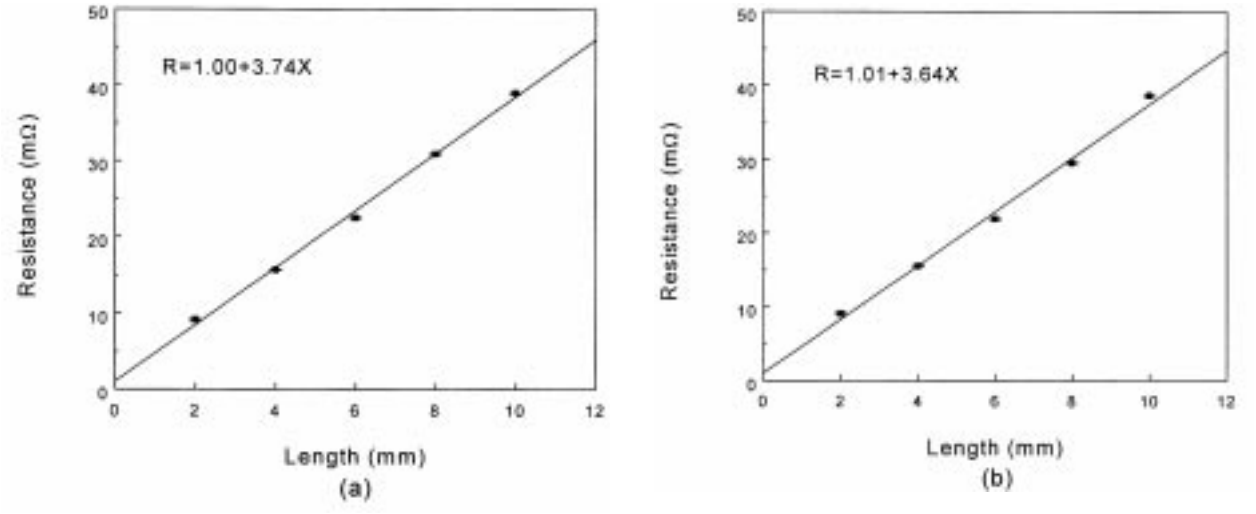

Figure 11 Resistance of various solder joints (a) 42Sn-58Bi/PtAg, (b) SnBi-1Cu/PtAg joint versus different length, which is indicated as X in Fig. 1a.

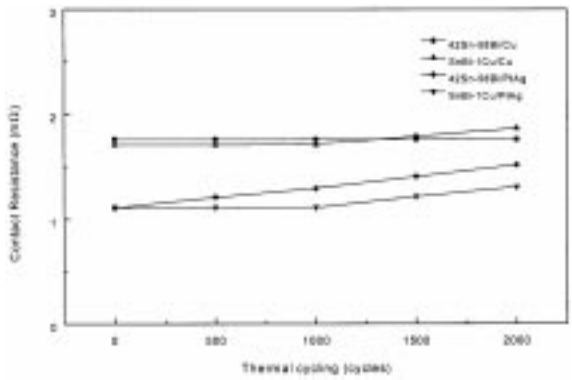

Figure 12 Contact resistance for 42Sn-58Bi/Cu, SnBi-1Cu/Cu, 42Sn-58Bi/PtAg and SnBi-1Cu/PtAg interfaces after 2000 thermal cycles.

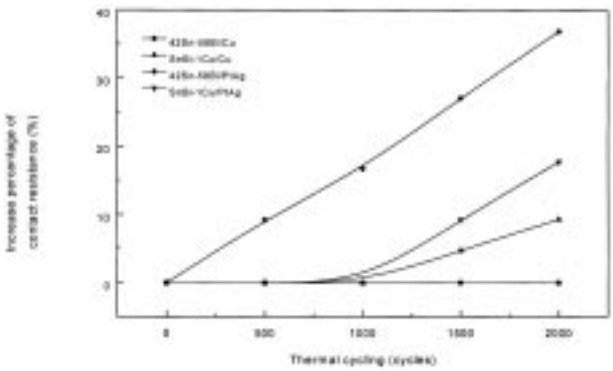

Figure 13 Change in contact resistance for 42Sn-58Bi/Cu, SnBi-1Cu/Cu, 42Sn-58Bi/PtAg, and SnBi-1Cu/PtAg interfaces after 2000 thermal cycles.

different thermal expansion coefficients. Thermal fatigue cracks usually nucleate at the edge of the solder fillet, and then propagate along the solder/conductor interface. Portions of cracks, however, go through the Al_2O_3 substrate. The thermal cycling induced substrate cracking is caused by stress concentration and the brittle nature of the ceramic substrate.

3. Contact resistance of the eutectic Sn-Ag/Cu joint does not increase appreciably after thermal cycling. The solder joints of the 42Sn-58Bi/Cu, the SnBi-1Cu/Cu, the 42Sn-58Bi/PtAg, and the SnBi-1Cu/PtAg maintain their integrity after 2000 thermal cycles due to the negligible increase in the contact resistance.

Acknowledgments

The authors are grateful for the financial support from the National Science Council, Taiwan under the contract No. NSC 86–2221-E-007–043.

References

1. S. K. KANG and A. K. SARKHEL, *J. Electron. Mater.* **23**(**8**) (1994) 701.
2. K. C. LIU and J. G. DUH, *IEEE Trans. Compon. Hybrids Manuf. Technol.* **14**(**4**) (1991) 703.
3. C. MELTON, *IEEE* (1993) 1008.
4. P. T. VIANCO, A. C. KILGO and R. FRANT, *J. Electron. Mater.* **24**(**10**) (1995) 1493.
5. M. MCCORMACH and S. JIN, *JOM* (1993) 36.
6. M. E. LOOMANS, S. ZAYNMAN, G. GHOSH and M. E. FINE, *J. Electron Mater.* **23**(**8**) (1994) 741.
7. C. A. MACKAY and W. D. VON VOSS, *Mater. Sci. Technol.* **1** (1985) 240.
8. S. JIN and M. MCCORMACK, *J. Electron. Mater.* **23**(**8**) (1994) 735.
9. L. E. FELTON, C. H. RAEDER and D. B. KNORR, *JOM* (1993) 28.
10. J. GLAZER, *J. Electron. Mater.* **23**(**8**) (1994) 693.
11. C. H. RAEDER, L. E. FELTON, V. A. TANZI and D. B. KNORR, *J. Electron. Mater.* **23**(**7**) (1994) 611.
12. ARAKI, A. M. JACKSON and P. T. VIANCO, *ibid.* **23**(**8**) (1994) 757.
13. E. P. WOOD and K. L. NIMMO, *ibid.* **23**(**8**) (1994) 709.
14. C. H. RAEDER, L. E. FELTON, D. B. KNORR, G. B. SCHMEELK and D. LEE, Proceedings of the IEEE/CHMT International Electronics Manufacturing Technology Symposium (1993) 119.
15. W. J. TOMLINSON and I. COLLIER, *J. Mater. Sci.* **22** (1987) 1835.
16. Z. MEI and J. W. MORRIS, JR., *J. Electron. Mater.* **21**(**6**) (1992) 599.
17. M. MCCORMACK, S. JIN and G. W. KAMMLOTT, *IEEE Trans. Compon. Packaging Manuf. Technol. A* **17**(**3**) (1994) 452.
18. Y. Y. WEI and J. G. DUH, *J. Mater. Sci.* **9** (1998) 373.
19. J. HAIMOVICH, *Welding Research Supplement* (1989) 102.
20. T. LYMAN, ''The Ninth Edition of Metals Handbook'', Vol. 9, (American Society for Metals, 1985) p. 126.

21. M. C. PECHT, ''Soldering Processes and Equipment'' (John Wiley & Sons Inc., New York, 1993) ch. 6.
22. G. K. REEVES and H. B. HARRISON, *IEEE Electron Device Letters* **EDL-3(5)** (1982) 111.
23. R. L. KEUSSEYAN, P. T. GOELLER, L. E. DELLIS, J. R. THRASH, T. G. DAVENPORT and R. F. HAZELWOOD, *ISHM '90 Proceedings*, (1990) 199.
24. R. L. KEUSSEYAN, P. T. GOELLER, L. E. DELLIS, J. R. THRASH, T. G. DAVENPORT and R. F. HAZELWOOD, *ibid*. (1990) 190.
25. T. LYMAN, ''The Eighth Edition of Metals Handbook'', Vol. 1, (American Society for Metals, 1985) p. 48.
26. J. SEYYEDI, *J. Electron. Packaging* **115** (1993) 305.

Received 6 January
and accepted 16 June 2000